Harmonic patterns embedding ictal EEG signals in focal epilepsy: a new insight into the epileptogenic zone

Lingli Hu,[1] Lingqi Ye, [1] Hongyi Ye, [1] Xiaochen Liu,[2] Yuanming Zhang,[2] Zhe Zheng,[3] Hongjie Jiang,[3] Cong Chen,[1] Zhongjin Wang,[1] Junming Zhu,[3] Zhong Chen,[4] Dongping Yang*,[5] Shuang Wang*[1]

1. Department of Neurology and Epilepsy Center, Second Affiliated Hospital, School of Medicine, Zhejiang University, Hangzhou, China
2. College of Information Science and Electronic Engineering, Zhejiang University, Hangzhou, China
3. Department of Neurosurgery, Second Affiliated Hospital, School of Medicine, Zhejiang University, Hangzhou, China
4. Key Laboratory of Neuropharmacology and Translational Medicine of Zhejiang Province, School of Pharmaceutical Sciences, Zhejiang Chinese Medical University, Hangzhou, China
5. Research Center for Human-Machine Augmented Intelligence, Research Institute of Artificial Intelligence, Hangzhou, China

*Correspondence to：

Shuang Wang*

Department of Neurology, Second Affiliated Hospital, School of Medicine, Zhejiang University, Hangzhou 310009, China; E-mail: wangs77@zju.edu.cn

Dongping Yang*

Research Center for Human-Machine Augmented Intelligence, Research Institute of Artificial Intelligence, Zhejiang Lab, Hangzhou 311100, China; E-mail: dpyang@zhejianglab.com

Key Words: Harmonic pattern, epileptogenic zone, nonlinear phenomena, epilepsy surgery.

Abstract

The ictal EEG biomarkers of the epileptogenic zone (EZ) need to be better defined. The power and structure of ictal fast activity are important in EZ localization, but EEG onset patterns are heterogeneous and initial fast activity is absent in many patients. Here we defined a unique spectral structure of "harmonic pattern" (H pattern) on stereo-EEG (SEEG), characterized by multiple equidistant, high-density bands with varying frequency on time frequency map. H pattern was commonly observed among 57 (81.4%) out of 70 patients with focal onset pattern on SEEG. It was presented in seizures with various ictal onset patterns with or without fast activity, and during early or late stage of seizures. H pattern usually expressed at very close time point across the seizure onset zone (SOZ), primary propagation zone and sometimes other areas, with the same fundamental difference, reflecting an inter-regional synchronization within the ictal network during this time. Notably, SOZ showed the highest proportion of channels expressing H-pattern, and also highest band number of H-pattern. At patient level, the dominant H pattern was defined as those with high rank in band numbers (the third quartile, Q3). Resection of the region expressing dominant H pattern, but not SOZ, independently predicted seizure freedom after surgery, suggesting it is an ictal marker of EZ. How H pattern was produced was then investigated. It only embedded into two types of EEG segments: fast activity with a frequency >25Hz (FA-H pattern) at early seizure propagation (mean 13.3 sec after onset), and irregular polyspikes (> 5 Hz, PS-H pattern) during late propagation (mean 23.3 sec after onset). Nonlinear analysis was used to unravel the mechanism

underlying H pattern generation. Our data showed it was produced by specific nonlinear phenomena rather than intermodulation of frequencies or purely methodological artefact. The nonlinearity was stronger for dominant compared to non-dominant H pattern. According to the spectral parameters, we postulate that FA-H pattern may be supported by a predominant and synchronized firing of GABAergic neurons, while excitatory neuron firing is more important for PS-H pattern. As a distinctive and common ictal spectral feature, H pattern conveys unique information of ictal neural dynamics and provides new insights into the EZ. Our study also provides evidence that there is an elongated time-window to measure EZ using quantitative EEG.

Introduction

The epileptogenic zone (EZ), defined as the site of primary organization of ictal discharge, refers to the areas of excessive synchronization at seizure onset. [1] Whether the EZ is completely removed determines the surgical outcome for drug-resistant focal epilepsy. Intracranial electroencephalography (iEEG) provides the best precision for EZ localization, especially for MRI-negative epilepsy.[2] Currently, clinical analyses of iEEG largely depend on visual inspection. Ictal patterns on iEEG are highly heterogeneous in terms of onset morphology, evolution and propagation, suggesting a complex, highly dynamic and individualized nature of ictal network.[3] Interpretation of iEEG is inevitably subject to personal or institutional experience. Among those performed iEEG evaluation and subsequent resective surgery, about 50-70% of the patients are able to finally achieve prolonged seizure freedom [4,5]. The overall outcome of resective epilepsy surgery in focal epilepsy remains unsatisfactory, even for those with focal onset pattern on iEEG.

In recent decades, many quantitative EEG methods are created to optimize EZ definition in addition to traditional visual inspection.[6] Analysis of interictal high frequency oscillations (HFOs) together with spikes on wide-band EEG recording is useful to delineate the boundary of EZ.[7-9] Among the studies of ictal EZ markers, most methods utilize fast activity (FA) alone or in combination with other features.[10-13] Presence of focal ictal fast activity is found to be consistently correlated with favorable surgical outcome in neocortical epilepsy.[14] The epileptogenic index, which examines alterations in the energy ratio between fast activity (mostly in gamma

range) and slow activity involved at early seizure onset in a specific region, provides quantitative measurement for epileptogenic network.[10] Epileptogenicity mapping can visualize such ictal EEG change in energy ratio using statistical parametric mapping software.[11] Additionally, analyzing alteration in functional connectivity of the ictal low-voltage fast activity also provides complementary information for EZ localization.[15,16] However, these methods are usually based on measuring fast activity > 30Hz, but not efficient for slower EEG onset patterns that account for 20-30% of common onset patterns on iEEG.[17-19] Nowadays we are still on the way to optimize ictal biomarkers of EZ.

Recently, the concept of EEG fingerprint is proposed as an ictal EZ marker based on a highly selected cohort.[20,21] It includes three concurrent features in specific cortical regions: pre-ictal spiking, multiple-band fast activity, and simultaneous low-frequency suppression. One key finding is that the structural property of the ictal fast activity is as important as its powers. On time-frequency maps (TFM), the ictal fast activity is consisted of multiple narrow bands instead of broad-band activity. Notably, the identified narrow band activity mainly contains gamma or ripple oscillations, and sometimes in beta or even alpha oscillations. The phenomenon of ictal narrow band activities may be common in focal epilepsy and deserves further study.

Here we extensively explore the spectral property of ictal iEEG on TFM in focal epilepsy, with an aim to better clarify the clinical relevance of multi-band fast activity for EZ localization. We identified a unique and common spectral structure of

"harmonic pattern" (H pattern), characterized by multiple equidistant, high-density bands with varying frequency overtime. The characteristics of the initial H pattern and its clinical relevance were investigated in a cohort of focal epilepsy who underwent iEEG evaluation. Our data reveals H pattern is not purely generated by methodological effect but harbors biological information important for EZ localization, because resection of the area expressing the feature was correlated with surgical outcome. H pattern on ictal EEG is not an isolated phenomenon, similar harmonic patterns harboring biological meaning can be observed in other aspects of clinical neurophysiology. In this study, we also explored the mechanism underlying H pattern generation using nonlinear analysis.

Methods

Patients and stereo-electroencephalography evaluation

We reviewed consecutive patients with drug-resistant focal epilepsy who underwent stereo-electroencephalography (SEEG) evaluation and subsequent resective surgery in our epilepsy center between January 2014 and April 2021. They were all followed-up for > 2 years after surgery. A comprehensive evaluation was conducted, including a detailed medical history, neuropsychological testing, neuroimaging examination, and scalp video-EEG recordings. This study was approved by the Medical Ethics Committee of the Second Affiliated Hospital, Zhejiang University School of Medicine (Study No. 2020-910). SEEG was performed using intracerebral multiple-contacts electrodes, with contacts that were 2 mm in

length, 0.8 mm in diameter, and 1.5 mm apart. SEEG signal was recorded by EEG systems with 256 channels (Nihon Kohden) or 128 channels (Xltek, Natus, Ontario, Canada) at a sampling rate of 1000 or 2000 Hz. Pre-implantation magnetic resonance imaging (MRI) and post-implantation computed tomography (CT) were co-registered to locate each contact anatomically along each electrode trajectory.

EEG data were reviewed on bipolar montage. Only contacts within the grey matter were selected. The seizure onset pattern (SOP) was assessed on the earliest involved electrodes. As previously described,[8,15,22] the SOZ was defined as the area unequivocally showing the earliest change on iEEG, and early propagation zone (PZ) as the area showing a rapid spread of ictal activity within 3-5 seconds of seizure onset. Other brain regions were classified as other zone (OZ). The SOP, SOZ, PZ and OZ were independently defined by at least two clinical neurophysiologists. In case of inconsistence, they would discuss with a third epileptologist to reach a consensus.

Surgical plans were made by a multidisciplinary team independently of this study. After surgery, preoperative MRI and postoperative CT were fused to identify exact borders of resection. The electrode contacts located on the border of resection margins or in disconnected tissues were defined as removed contacts. Surgical outcomes were assessed at the latest follow-up according to Engel's classification. Surgical outcomes were classified as Engel 1a (seizure free, SF) and Engel >1a (not seizure free, NSF).

Quantitative EEG analysis

Identification of Harmonic patterns

All analyses were based on bipolar signals recorded from artifact-free channels. For each seizure, a window of 110 s of SEEG data was extracted: 10 s before and 100 s after the seizure onset, and a 110 s-epoch of SEEG data was also collected (>2 min before the seizure onset) as a statistical baseline. Morlet wavelet transform analysis was used to produce TFM and further validated by multitaper method. Both methods used linear spacing in the frequency range of 1 to 300 Hz with an interval of 1Hz. The baseline TFM was used to normalize the seizure data TFM whose power at each frequency was divided by the corresponding baseline power (for methodological details, see Olesya Grinenko, et al., 2018).[20]

H pattern was identified using following features: multiple equidistant high-density, narrow bands with changing frequency over time (Fig. 1C). The frequency bands of H pattern for each pair of channels, from low to high, were referred to as the first (f_{1st}), second (f_{2st}), third frequency band (f_{3st}), and so on. At a particular time point, the difference between two adjacent frequency bands was defined as the frequency interval, which is equal to the fundamental frequency (f). The frequencies of narrow bands fall around the multiples of the fundamental frequency. That is, f_{nst}= n f (f_{1st}=f; f_{2st}=2f; f_{3st}=3f; f_{3st}=3f ;….). The minimal and maximal frequencies were determined at peaks of the first and last frequency bands, respectively. Usually this minimal frequency equaled fundamental frequency. The parameters of H pattern, such as

minimal/maximal frequencies and start/end time were extracted in Brainstorm software. For each patient, H pattern was identified in one selected habitual seizures. If several H patterns were consecutively presented in a single seizure, only the earliest occurring one was selected for analysis.

To further identify channels with the dominant H pattern, a threshold of Q3 was set, given as the upper quartile (75th percentile of data distribution) of the total band number:

$$Q3 = (n + 1) \times 3/4, \quad (1)$$

where n is the highest band number in each individual. Any channel with a band number of the H pattern exceeding this threshold were marked as a “dominant-H pattern” (*d*H pattern) channel, otherwise it was labeled as a "non-dominant H pattern” (non-*d*H pattern) channel.

Correlation between removal of region expressing *d*H pattern or SOZ and postoperative outcome was analyzed. Resection ratio was calculated as the number of channels with the events included within the resection over the total channel number of the events. A value of 1 identifies a completely removal of the events; whereas a value of 0 represents complete non-removal.

Nonlinear analysis of H pattern

As TFM is produced by Morlet wavelet transforming the detrended SEEG signals, all information as well as features such as H pattern can be rooted in their waveshapes. Generally, harmonic generation can be attributed to various factors, including

nonlinear effects (e.g., impulses in a signal, waveshape distortion, etc.) and intermodulation of different frequencies. Physically speaking, the primary cause of harmonic generation stems from the nonlinear effects. For instance, as demonstrated in (Supplementary Fig. 2-3, H pattern can be generated by various nonlinear transforms of a single frequency sinusoidal oscillation, resulting in distorted waveshapes ((Supplementary Fig. 3).

Identifying the distorted waveshape of the SEEG signals accounting for H pattern was crucial in understanding the neural mechanism underlying the generation of H pattern. To this end, the original SEEG signals were carefully analyzed. Firstly, the original signals were detrended using the smoothing method 'loess' in MATLAB to render the waves oscillating around a zero-valued baseline, which separated the waves into troughs and peaks. Then, a sinusoidal wave with a single frequency was employed to fit each trough and peak. Finally, specific waveshape distortion can be investigated and identified for each H pattern by comparing the frequencies of troughs and peaks as well as its primary component of the original signal, as detailed in Fig. 5-6.

Bicoherence and cross-frequency amplitude-amplitude coupling analysis of H pattern

Harmonic structure may also be generated by intermodulation of different frequencies: In a phase-amplitude coupled (PAC) signal, the phase coupling of the modulation frequency (f_m) to the carrier frequency (f_c) results in the appearance of

amplitude-modulated side-peak, which are usually the carrier frequency plus or minus the modulation frequency, i.e., (f_c $\pm f_m$). If f_m = f_c - f_m, which would give similar harmonic results (f_m, $2f_m$, $3f_m$).

In order to distinguish between the harmonic structures due to PAC and nonlinear effects as reflected in the distorted waveshapes, we employed bicoherence method and cross-frequency amplitude-amplitude coupling (AAC), which are commonly used to characterize nonlinearity in dynamical system and dissociate the harmonic and non-harmonic PAC of EEG or MEG signals.[23] The relative strength of bicoherence and AAC peaks allows for dissociating harmonic and non-harmonic PAC, as bicoherence and AAC between the base frequency and its harmonics imply the harmonic structures from a single nonlinear oscillator[23].

Bicoherence can be estimated according to the following formula with the normalization factor[24]:

$$\mathrm{b}(f_1, f_2) = \frac{|\sum_n \mathrm{F}(f_1)\mathrm{F}(f_2)*\mathrm{F}(f_1+f_2)|}{\sum_n |\mathrm{F}(f_1)\mathrm{F}(f_2)*\mathrm{F}(f_1+f_2)|} \qquad (2)$$

where $\mathrm{b}(f_1,\ f_2)$ describes the phase coupling degree among three waves with a frequency of f_1, f_2, and $f_1 + f_2$, respectively, with a near-one value denoting strong coupling but a near-zero value denoting weak or even no coupling; F(f) is the Fourier transform of the signal, and * denotes the complex conjugate. AAC can be estimated by the Pearson correlation coefficients between amplitude time-series of two filtered time series at frequencies f_1 and f_2, respectively, which were derived from Hilbert transformation .

In our study, EEG signals of H pattern were divided into epochs (1/10 signal length) with 50% overlap, resulting in 19 epochs. Bicoherence values were computed in all frequency pairs (0-250 Hz, 0.25 Hz intervals), generating the wavelet bicoherence matrix, b. Each element, b(f_1, f_2), represents bicoherence value at bifrequency pair (f_1, f_2) where 0≤f_1, f_2≤250 Hz. To ensure statistical significance, 100 surrogated data were created using phase randomization, preserving spectral content and linear properties. A 99% statistical threshold was defined as mean plus three standard deviations of surrogated bicoherence estimates at each frequency pair. Only values above the threshold were considered significant for further analysis.

The AAC was performed by calculating the Pearson correlation coefficient between the amplitude time series derived from the linearly constrained minimum variance (LCMV)-beamformed Fourier time series, where the amplitude time series are in the frequency range of f_1 (0.5 to 250 Hz) and f_2 (0.5 to 250 Hz) with a step size of 0.5 Hz.

To facilitate statistical analyses, we defined six regions of interest (ROIs) in the bicoherence frequency map, which represent all possible intersections of the first three frequency bands (Fig. 7C). Higher number of frequency bands was not considered because most H pattern channels have no more than three frequency bands. A total of 10 representative patients from five brain regions (temporal, frontal, parietal, occipital, and opercular/insular; 2 for each region) were selected for statistical analysis.

Statistical analysis

SPSS 24.0 software was used for statistical analysis. All continuous variables were first tested using a homogeneity test for variance and a test of normality. According to the results, normal variables were presented as mean ± standard deviation (SD); and non-normal variables were reported as medians (interquartile range). Categorical variables were expressed as frequencies. Comparisons between two groups were made using Student's t tests or nonparametric Mann-Whitney U tests, and comparisons among three groups were analysed with one-way analyses of variance (ANOVAs) or nonparametric Kruskal-Wallis tests. Chi-square tests were used for categorical variables. Multivariate logistic regression was used to control for potential confounding factors when comparing *d*H pattern resection ratio between the two groups. A P value < 0.05 was considered statistically significant.

Results

Patients and iEEG evaluation

We reviewed SEEG data from all patients who were evaluated with SEEG between January 2014 and April 2021 (N = 80). Of these, three were excluded because of insufficient clinical and EEG information, and other seven because of non-localizable origin. Among 70 patients who were included, all seizures were classified into 6 seizure onset patterns (Fig. 1A):

Pattern 1, 36 cases with preictal spikes/sharps/polyspikes following fast activity > 14Hz (low-voltage fast activity (LVFA), amplitude < 30μV pattern 1.1; high-voltage fast activity (HVFA), amplitude ⩾30μV, pattern 1.2);

pattern 2, 10 cases with slow wave/ DC shift followed by LVFA;

pattern 3, 12 with spikes activity;

pattern 4, seven with LVFA;

pattern 5, three with beta activity;

pattern 6, one with delta-brush.

After follow-up for 35.5 ± 21.3 months 48 patients (68.6%) achieved seizure freedom.

Fifty-seven of the 70 patients presented with at least one H pattern, and the other 13 patients were absence of discernable H pattern throughout ictal periods. Notably, without TFM, direct visual inspection could hardly discern the EEG segments harboring H pattern from the counterparts without H-pattern. H pattern was presented in all SOPs except delta-brush (Figure. 1A and B), which was found in only one patient. Between the H pattern and non-H pattern groups, no differences were found for SOP (P = 0.061, chi-square test), lobar origin (P = 0.517, chi-square test), presence of MRI lesion (85.9 % versus 76.9%, P = 0.416, chi-square test) or seizure freedom (68.4 % versus 69.2 %, P = 1.000, chi-square test). The most common pathological finding was focal cortical dysplasia II (FCD II) in both groups (49.1 % versus 38.5 %, chi-square test). Finally, 57 (81.4%) patients were included in further analysis of H pattern (Table 1). The EZ fingerprint, as defined by Grinenko's methods, was observed in 25 out of the 70 (35.7%) patients. Among the 57 patients recorded

with ictal H pattern, there were 31 males and 26 females. The mean age at epilepsy onset was 10.4 ± 8.5 years. The mean age of the patients at surgery was 23.6 ± 12.3 years. The mean number of contacts per patient was 94.7±29.1. Forty-nine patients (85.9 %) exhibited identified or subtle lesions on MRI. The most common seizure origins were the frontal and temporal lobes. FCD type II was the most common pathological finding (49.1%). At final follow-up 39 patients (68.4%) achieved seizure freedom (Table 1). No difference in various features was found between the seizure free and non-seizure free groups except pathological findings.

Classification of H pattern

The initial H pattern appeared 18.1 ± 20.5 s after the ictal EEG onset on TFM. Its onset time was not limited to early seizure evolution, but sometimes extended to late stage of seizures (Fig. 1C). H pattern consistently coexisted with two certain EEG patterns: fast activity > 25 Hz and irregular polyspikes > 5 Hz. Accordingly, H patterns were classified into two types: FA-H pattern and PS-H pattern (Fig. 2A). For the first H pattern observed, their proportions were close (FA-H pattern, 30/57; PS- H pattern, 27/57). Less number of bands (3 (4.25) vs 6 (8.5), $P = 0.006$, nonparametric Mann-Whitney U test) and higher frequency interval (47.5 (56.75) vs 15 (20) Hz, $P < 0.000$, nonparametric Mann-Whitney U test) was found for FA-H pattern compared with PS-H pattern. Additionally, in FA-H pattern the start time (5.2 (18.19) vs 18.7 (17.2) s, $P = 0.004$, nonparametric Mann-Whitney U test) and end time (25.4 (28.3) vs 33.9 (11.7) s, $P = 0.015$, nonparametric Mann-Whitney U test) was earlier than PS

pattern; and the minimal frequency (60 (54.7) vs 15(20) Hz, $P < 0.000$, nonparametric Mann-Whitney U test) and maximal frequency (193 (120.75) vs 126 (159) Hz, $P = 0.021$, nonparametric Mann-Whitney U test) were higher (Fig. 2B). In all H patterns, the frequencies of bands varied over time: their bands went upwards, downwards, or were bell-shaped and then vanished.

Spatial distribution of H pattern

H pattern commonly occurred in SOZ, PZ and sometimes in OZ at very close time point, with almost the same frequency interval, even if these regions were remotely separated. The end time and minimal/maximal frequencies of H pattern were not different across regions. Sometimes the H pattern even extended to the ipsilateral thalamus, occurring simultaneously with the cortical regions and showing the same frequency interval (Supplementary Fig. 1).

The proportion of the contacts showing H pattern in each region decreased in order from SOZ, PZ to OZ (SOZ vs PZ, $P < 0.001$; SOZ vs OZ, $P < 0.001$; PZ vs OZ, $P < 0.001$, Paired Wilcoxon signed-rank, after Bonferroni correction). The highest number of bands was in SOZ (SOZ vs PZ, $P = 0.03$; SOZ vs OZ, $P = 0.03$, Paired Wilcoxon signed-rank, after Bonferroni correction, Fig.3C).

Dominant H pattern and surgical outcome

The H pattern of most SOZ showed the highest numbers of bands (Fig. 3C). To define H pattern potentially marking epileptogenicity, we defined the *d*H pattern

regions using Q3 as a threshold in each patient. Patients with seizure freedom after surgery had a significantly higher proportion of the *d*H pattern-expressing areas than those seizure recurrences ($P < 0.001$, nonparametric Mann-Whitney U test). No such difference was found in the SOZ ($P = 0.966$, nonparametric Mann-Whitney U test) (Fig. 4A). The start and end time of the *d*H pattern were not statistically different between two groups. On multivariate analysis, after adjusting for potential confounders of pathology, presence of MRI lesion, and epilepsy duration, a complete resection of areas expressing the *d*H pattern was significantly associated with a chance of seizure freedom (Fig. 4B).

EEG waveshapes accounting for H pattern

By analyzing the EEG waveshapes of *d*H and non-*d*H patterns for both types of H pattern, the results showed that FA-H pattern can be generated by diverse waveshapes, including sharper troughs, sharp extended troughs and peaks, asymmetric waveshapes, and phase-locked high gamma amplitude, while PS-H pattern was mainly caused by rhythmic pulses. In the following, four cases of FA-H pattern and one case of PS-H pattern were selected as representatives and investigated in details.

The first one accounting for FA-H pattern was the waveshape with sharper troughs, as presented in Fig. 5, left panel. The original signals, detrended signals and corresponding TFMs with clear harmonic patterns (Fig. 5A and D) showed the higher power of harmonic components but the lower power of the primary component in *d*H pattern compared to those in non-*d*H pattern. The sinusoidal waves were then

employed to fit troughs and peaks, with the corresponding fitted periods and TFMs (Fig. 5B and E). The strong harmonic components in *d*H pattern was due to the sharp troughs (Fig. 5B middle and demonstration in Supplementary Fig. 3A), while the weaker harmonic components in non-*d*H pattern was due to the period fluctuation of both troughs and peaks (Fig. 5E, middle). The point was also supported by the distribution of fitted periods of both troughs and peaks, and their consequent pairs (Fig. 5C and F).

The second one was the waveshape with sharp extended troughs and peaks (Fig. 5G, right panel). The harmonic components in the low frequency region (<150Hz) are dominated by the 1rd and 3th order of the primary frequency (Fig. 5G bottom). The results showed that the sinusoidal waves were sharp with short periods than the primary period of the EEG signal in *d*H pattern (Fig. 5H, middle). Correspondingly, the sharp sinusoidal waves in *d*H pattern are extended with more than half of the primary period (Fig. 5I), as demonstrated in Fig. 5I bottom where the ratio of durations of both troughs and peaks over the primary period was much larger than half, and the simple case in Supplementary Fig. 3B. In contract, this effect was much reduced in non-*d*H pattern (Fig. 5L bottom).

The third one was the asymmetric waveshape (Fig. 6, left panel). The results showed that *d*H pattern exhibited stronger harmonic components than those of non-*d*H pattern. The sinusoidal wave fitted signals also showed much stronger harmonic components of *d*H pattern than those of non-*d*H pattern (Fig. 6B and E, bottom). It could be explained by another feature: asymmetric waveshape with longer

trough-to-peak durations than peak-to-trough durations (Fig. 6C and F), and demonstrated by a simple case presented in Supplementary Fig. 3C.

The fourth FA-H pattern was similar to that in the previous study,[25] with EEG of *d*H pattern and non-*d*H pattern presented as Supplementary Fig. 4. The *d*H pattern showed the similar features with those in the ictal core with strong high gamma (80-150 Hz), while the non-*d*H pattern presented similar features with those in the penumbra of Weiss's study. Stronger harmonic components in *d*H pattern is due to an increased high gamma at the peak of the lower frequency rhythm (4-30 Hz, Weiss, et. al., 2013). Such kind of phase-locked high gamma amplitude happened at the onset of LVFA, and before the emergence of the clear H pattern (Supplementary Fig. 4).

The waveshape accounting for PS-H was the sharp rhythmic pulses (Fig. 6, right panel). The main difference between *d*H pattern and non-*d*H pattern lied in the rhythmic pulses, whose removal significantly reduced the power of harmonic components in *d*H pattern (Fig. 6H), and rendered the rest EEG signals of *d*H pattern similar to those of non-*d*H pattern (Fig. 6H and K). The harmonic components could be further reduced by sinusoidal wave fitting of troughs and peaks (Fig. 6I and L). Additionally, the rest EEG signals of *d*H pattern had larger amplitude than those of non-*d*H pattern, indicating that the region of non-*d*H pattern was driven by the activities in the region of *d*H pattern, whose sharp rhythmic pulses might be filtered out in the spatiotemporal signal propagation.

Distinguishing between the harmonic structures due to PAC and nonlinear effects

In 10 representative cases, the results show that the observed harmonic pattern ware attributed to nonlinear effects and not to the PAC (Fig. 7): The presence of multiple peaks of bicoherence and AAC between the fundamental frequency and its harmonics. .

Next, we compared the difference in the mean of the maximum bicoherence values of the *d*H pattern and the non-*d*H pattern. The results showed that all ROIs demonstrated higher bicoherence in the *d*H patterns compared to the non-*d*H patterns (nonparametric Mann-Whitney U test),. It suggests that the coupling between frequency bands in *d*H pattern is stronger than that in non-*d*H pattern (Fig. 7D). This result is consistent with SFig. 4.

Discussion

As a distinct feature on TFM recorded in ictal SEEG signals, H pattern and its correlation with epileptogenic zone were systematically investigated in this study. H pattern was commonly present in most patients with various EEG onset patterns, either during early or late seizure propagation. Moreover, despite the morphology and parameters of H pattern varied greatly across individuals, each patient had highly uniform pattern for all habitual seizures, suggesting that it represents an individualized inherent property of epileptogenic network. H pattern was spatially co-localized within the epileptic zones of SOZ and PZ, which exhibited the highest

numbers of bands as well. Furthermore, a complete resection of cortical regions expressing dominant H-patterns, but not SOZ, independently predicted seizure freedom after resection surgery in our cohort of focal onset epilepsy, indicating the dominancy of H pattern could be a promising and universal ictal marker of the EZ. Our study also revealed that H pattern can be linked to diverse waveshapes. This reflects nonlinear features in the seizure, indicating diverse underlying neuronal mechanisms, harboring clinical significance rather than intermodulation of frequencies or methodological artifact. When H patterns were expressed across different cortical regions, a uniformed fundamental frequency was observed, which reflected synchronized cortical firing as a key stage of seizure propagation. Analysis of H pattern not only provides important information of ictal neural dynamics, but also gives insights into the EZ as well.

Many quantitative methods have been developed to complement visual EEG analysis and help define EZ in an objective way. These methods usually measure the energy of ictal fast activity. Epileptogenicity index is calculated as the energy ratio between the fast frequencies (beta + gamma) and slow frequencies (theta + alpha).[10] David et al. (2011) aimed to identify the EZ based on the maximal frequency of FA during early seizure spread.[11] Gnatkovsky et al. (2014) found EZ could be defined by combined features at seizure onset: ictal fast activity at 80-120 Hz associated with polarizing shift and EEG flattening.[13] Our study strengthens that spectral property of ictal fast activity is pertinent to define EZ. Some of the FA-H patterns in our study are similar with narrow band fast activity with suppressed lower frequency activity

defined in EEG fingerprint study.[20] In addition, such highly-structured spectral feature was also observed during more late seizure propagation for PS-H patterns, sometimes in the seizures absent of initial fast activity. Our findings extend the concept of narrow band fast activity defined in study of EEG fingerprint and also suggest that the time window to define EZ using ictal EEG can be widened. In our cohort, the sensitivity to detect EEG fingerprint was 0.357, while ictal H pattern was common and its presence was independent of initial fast activity at seizure onset. In future, analysis of ictal H pattern on TFM is a practical method to complement other quantitative methods in defining EZ.

FA-H pattern and PS-H pattern occurred at different stages of seizure evolution. Unit recording studies in vivo and in brain slices disclose that different neuronal populations have distinct roles during seizure evolution. A typical partial seizure recorded with depth electrodes initiates with either low-voltage fast activity or "hypersynchronous" potentials, followed by irregular spiking, which eventually evolves into rhythmic bursts.[26] Robust evidences show that low-voltage fast activity is supported by a prominent activation of inhibitory interneurons and transiently shut off of excitatory cells.[27-32] Consequently, irregular spiking is associated with reduced inhibitory interneuron firing and increased excitatory interactions between excitatory neurons. The bursting activity at the terminal phase is characterized by the enhancement of both interneurons and excitatory neurons.[33] Accordingly, FA-H pattern may be dominated by inhibitory interneurons, whereas excitatory neuron firing plays a more important role in the PS-H pattern.

Neural oscillations are a prominent feature of brain recordings and are commonly associated with pathological and normal behaviors such as epileptic seizures, sleep, perception, and cognition.[34,35] In spectral analysis, it is common to filter the signals into certain frequency bands of interest. This approach processes the EEG signals as sinusoidal signals by default, smoothing the signals. However, some fine features of waveshapes may also be alteredor removed as well. There is growing evidence that neural oscillations are often non-sinusoidal. Waveshape characteristics of non-sinusoidal signals, such as general shape, sharpness, and rise-to-decay asymmetry,[36,37] are likely to be relevant to the underlying physiology.[37,38] Here we showed that specific waveshapes can account for the observed H pattern (Fig. 5-6 and SFig. 2-3) in the different patients, as well as discriminating *d*H pattern from non-*d*H pattern. For FA-H pattern, harmonics in *d*H pattern are generated by sharper troughs or/and peaks, asymmetric waveshapes, and even the phase-locked high gamma amplitude at specific phases (negative or positive peaks) of the low-frequency rhythm (Fig. 5 and Supplementary Fig. 4). For PS-H pattern, harmonics in *d*H pattern are generated by a more consistent waveshape, mainly the sharp rhythmic pulses (Fig. 6). It has been pointed out above that synchronization of interneurons to account for FA-H pattern and that of excitatory neurons for PS-H pattern. In FA onset, the synchronization level of interneurons evolves with the surrounding ion concentrations, particularly the extracellular potassium $[K^+]_o$ due to the increasing interneurons' hyperactivity. Such coevolving system with neuronal synchronization and quickly changing ion environment are full of complex nonlinear interactions, which underlie

the emergence of various brain oscillations as well as the H pattern discovered here. Taken together, our results disclose the role of nonlinear phenomena in EEG dynamics during seizures and contribute to a more comprehensive understanding of the ictal network. The strength of such non-linear interactions orchestrates certain physiological and pathological functions, and is also able to mark epileptogenicity as well. Further research is necessary to figure out the corresponding cellular and dynamical mechanisms underlying various waveshapes which account for the observed H pattern. In contract, for PS onset, the synchronization of excitatory neurons is more straightforward, and thus the observed waveshape accounting for PS-H pattern is more consistent across different patients.

Harmonic phenomena are well established in fields of sonics and electric circuit.[40-42] Similar harmonic phenomena can be observed on EEG or local field potential signals, which may be related to specific brain functional state.[43,44] During NREM sleep, sleep spindles show harmonic phenomena whose parameters changes with sleep stages, reflecting a functional alteration in the thalamocortical reverberant network.[45] On steady-state visual evoked potentials, reflecting responses of the parietooccipital cortex to periodic light stimulation, show harmonics and subharmonics corresponding to the frequency of stimulus.[46] However, harmonic phenomenon has not received much attention in the field of epilepsy, even though it has commonly been demonstrated in ictal EEG recording from animal models or patient.[47] [48,49] "Chirp signal" on ictal iEEG, defined as a spectral property with varying frequency content over time, was found to be co-localized with SOZ and very

analogous with H pattern.[49] This early study was performed on a small cohort containing 6 patients with focal epilepsy, and the parameters of the chirp signals remained unexplored. Currently, neither the biological significance of harmonic phenomena in epilepsy nor the mechanism underlying its generation is well understood. Moreover, it is usually taken as artifacts in clinic or in experimental studies. However, we argue that harmonic features harbor important information about the neural dynamics of seizures. Our study suggests that it can be linked to diverse nonlinear transforms of sinusoidal waves, and thus may be rooted to various underlying neuronal mechanisms. And this complex and varied mechanism exhibits a common feature-H pattern, suggesting that it may be a unique window for exploring the nature of epilepsy and its neural correlations.

In our study, H pattern shows narrowband oscillations rather than broadband oscillations. Narrowband oscillations reflect the synchronized firing of neuronal populations in the cortex.[50-52] We observed that the fundamental frequencies of the SOZ, PZ and OZ were the same during the H pattern, indicating synchronous neural firing across these regions. Surprisingly, such cross-regional synchronization in fundamental frequency can spread to very remote area, even contralateral cortical regions or subcortical region of the ipsilateral thalamus. H pattern reflects a very unique stage of seizure propagation. Notably, the *d*H pattern shows higher bicoherence values, which reflects stronger coupling. Our approach builds on previous efforts that have used bicoherence to aid the identification and characterization of harmonic structure. The results demonstrate that bicoherence can

not only quantify nonlinear features but also assist in distinguishing between *d*H pattern and non- *d*H pattern.

The study has several limitations. First, it is based on a cohort recruited from a single center, and its cellular mechanisms are not able to be investigated. Secondly, since morphology of H patterns are heterogeneous across subjects and currently not able to be automatically identified, its visual identification is inherently subjective to personal experience. Multiple H patterns may occur in the same seizure, and only the first occurrence of H patterns was analyzed in this study. H patterns which consecutively present require further analysis in the future. Thirdly, Q3 was used as the threshold defined the dominant H pattern. A patient-specific approach to define dominancy in H pattern may be necessary in future.

Conclusion

Our study defines a common and distinct ictal spectral feature of H pattern, which can be linked to specific underlying nonlinear mechanism. H pattern conveys unique information of ictal neural dynamics and gives new insights into the EZ. Our data also provides evidence that there is an elongated time-window to measure EZ using quantitative EEG.

Data availability

The data that support the findings of this study are available upon reasonable request from the corresponding author. The data are not publicly available to protect the privacy of research participants.

Competing interests

The authors have no conflicts of interest to disclose pertaining to this study.

Acknowledgements

This work was supported by the National Natural Science Foundation of China (grant numbers: 82171437, 82001365 and 82272112).

References

1. Bancaud J, Angelergues R, Bernouilli C, et al. Functional stereotaxic exploration (SEEG) of epilepsy. *Electroencephalogr Clin Neurophysiol.* 1970;28(1):85-86.
2. Jin B, So NK, Wang S. Advances of Intracranial Electroencephalography in Localizing the Epileptogenic Zone. *Neurosci Bull.* 2016;32(5):493-500.
3. Devinsky O, Vezzani A, O'Brien TJ, et al. Epilepsy. *Nature reviews Disease primers.* 2018;4:18024.
4. Sivaraju A, Hirsch L, Gaspard N, et al. Factors Predicting Outcome After Intracranial EEG Evaluation in Patients With Medically Refractory Epilepsy. *Neurology.* 2022;99(1):e1-e10.
5. He C, Chen C, Yang Y, et al. Clinical Characteristics and Prognostic Significance of Subclinical Seizures in Focal Epilepsy: A Retrospective Study. *Neurol Ther.* 2022;11(2):763-779.
6. Frauscher B. Localizing the epileptogenic zone. *Current opinion in neurology.* 2020;33(2):198-206.
7. Frauscher B, Bartolomei F, Kobayashi K, et al. High-frequency oscillations: The state of clinical research. *Epilepsia.* 2017;58(8):1316-1329.
8. Wang S, So NK, Jin B, et al. Interictal ripples nested in epileptiform discharge help to identify the epileptogenic zone in neocortical epilepsy. *Clin Neurophysiol.* 2017;128(6):945-951.

9. Wang S, Wang IZ, Bulacio JC, et al. Ripple classification helps to localize the seizure-onset zone in neocortical epilepsy. *Epilepsia.* 2013;54(2):370-376.

10. Bartolomei F, Chauvel P, Wendling F. Epileptogenicity of brain structures in human temporal lobe epilepsy: a quantified study from intracerebral EEG. *Brain.* 2008;131(Pt 7):1818-1830.

11. David O, Blauwblomme T, Job AS, et al. Imaging the seizure onset zone with stereo-electroencephalography. *Brain.* 2011;134(Pt 10):2898-2911.

12. Gnatkovsky V, Francione S, Cardinale F, et al. Identification of reproducible ictal patterns based on quantified frequency analysis of intracranial EEG signals. *Epilepsia.* 2011;52(3):477-488.

13. Gnatkovsky V, de Curtis M, Pastori C, et al. Biomarkers of epileptogenic zone defined by quantified stereo-EEG analysis. *Epilepsia.* 2014;55(2):296-305.

14. Wetjen NM, Marsh WR, Meyer FB, et al. Intracranial electroencephalography seizure onset patterns and surgical outcomes in nonlesional extratemporal epilepsy. *Journal of neurosurgery.* 2009;110(6):1147-1152.

15. Hu L, Xiong K, Ye L, et al. Ictal EEG desynchronization during low-voltage fast activity for prediction of surgical outcomes in focal epilepsy. *Journal of neurosurgery.* 2023;139(1):238-247.

16. Wilke C, Worrell G, He B. Graph analysis of epileptogenic networks in human partial epilepsy. *Epilepsia.* 2011;52(1):84-93.

17. Singh S, Sandy S, Wiebe S. Ictal onset on intracranial EEG: Do we know it when we see it? State of the evidence. *Epilepsia.* 2015;56(10):1629-1638.

18. Lagarde S, Buzori S, Trebuchon A, et al. The repertoire of seizure onset patterns in human focal epilepsies: Determinants and prognostic values. *Epilepsia.* 2019;60(1):85-95.

19. Balatskaya A, Roehri N, Lagarde S, et al. The "Connectivity Epileptogenicity Index " (cEI), a method for mapping the different seizure onset patterns in StereoElectroEncephalography recorded seizures. *Clin Neurophysiol.* 2020;131(8):1947-1955.

20. Grinenko O, Li J, Mosher JC, et al. A fingerprint of the epileptogenic zone in human epilepsies. *Brain.* 2018;141(1):117-131.

21. Li J, Grinenko O, Mosher JC, Gonzalez-Martinez J, Leahy RM, Chauvel P. Learning to define an electrical biomarker of the epileptogenic zone. *Hum Brain Mapp.* 2020;41(2):429-441.

22. Wang MY, Wang J, Zhou J, et al. Identification of the epileptogenic zone of temporal lobe epilepsy from stereo-electroencephalography signals: A phase transfer entropy and graph theory approach. *NeuroImage Clinical.* 2017;16:184-195.

23. Giehl J, Noury N, Siegel M. Dissociating harmonic and non-harmonic phase-amplitude coupling in the human brain. *Neuroimage.* 2021;227:117648.

24. Bullock TH, Achimowicz JZ, Duckrow RB, Spencer SS, Iragui-Madoz VJ. Bicoherence of intracranial EEG in sleep, wakefulness and seizures. *Electroencephalography and clinical neurophysiology.* 1997;103(6):661-678.

25. Weiss SA, Banks GP, McKhann GM, Jr., et al. Ictal high frequency oscillations distinguish two types of seizure territories in humans. *Brain.* 2013;136(Pt 12):3796-3808.

26. de Curtis M, Gnatkovsky V. Reevaluating the mechanisms of focal ictogenesis: The role of low-voltage fast activity. *Epilepsia.* 2009;50(12):2514-2525.

27. Velazquez JL, Carlen PL. Synchronization of GABAergic interneuronal networks during seizure-like activity in the rat horizontal hippocampal slice. *Eur J Neurosci.* 1999;11(11):4110-4118.

28. Köhling R, Vreugdenhil M, Bracci E, Jefferys JG. Ictal epileptiform activity is facilitated by hippocampal GABAA receptor-mediated oscillations. *J Neurosci.* 2000;20(18):6820-6829.

29. Ziburkus J, Cressman JR, Barreto E, Schiff SJ. Interneuron and pyramidal cell interplay during in vitro seizure-like events. *J Neurophysiol.* 2006;95(6):3948-3954.

30. Lasztóczi B, Nyitrai G, Héja L, Kardos J. Synchronization of GABAergic inputs to CA3 pyramidal cells precedes seizure-like event onset in juvenile rat hippocampal slices. *J Neurophysiol.* 2009;102(4):2538-2553.

31. Gnatkovsky V, Librizzi L, Trombin F, de Curtis M. Fast activity at seizure onset is mediated by inhibitory circuits in the entorhinal cortex in vitro. *Ann Neurol.* 2008;64(6):674-686.

32. Fujiwara-Tsukamoto Y, Isomura Y, Imanishi M, et al. Prototypic seizure activity driven by mature hippocampal fast-spiking interneurons. *J Neurosci.* 2010;30(41):13679-13689.

33. de Curtis M, Avoli M. Initiation, Propagation, and Termination of Partial (Focal) Seizures. *Cold Spring Harbor perspectives in medicine.* 2015;5(7):a022368.

34. Samarasinghe RA, Miranda OA, Buth JE, et al. Identification of neural oscillations and epileptiform changes in human brain organoids. *Nature neuroscience.* 2021;24(10):1488-1500.

35. Cole S, Voytek B. Cycle-by-cycle analysis of neural oscillations. *J Neurophysiol.* 2019;122(2):849-861.

36. Sherman MA, Lee S, Law R, et al. Neural mechanisms of transient neocortical beta rhythms: Converging evidence from humans, computational modeling, monkeys, and mice. *Proc Natl Acad Sci U S A.* 2016;113(33):E4885-4894.

37. Cole SR, Voytek B. Brain Oscillations and the Importance of Waveform Shape. *Trends Cogn Sci.* 2017;21(2):137-149.

38. Cole SR, van der Meij R, Peterson EJ, de Hemptinne C, Starr PA, Voytek B. Nonsinusoidal Beta Oscillations Reflect Cortical Pathophysiology in Parkinson's Disease. *J Neurosci.* 2017;37(18):4830-4840.

39. Stacey WC, Lazarewicz MT, Litt B. Synaptic noise and physiological coupling generate high-frequency oscillations in a hippocampal computational model. *J Neurophysiol.* 2009;102(4):2342-2357.

40. Schaefer MK, Kössl M, Hechavarría JC. Laminar differences in response to simple and spectro-temporally complex sounds in the primary auditory cortex of ketamine-anesthetized gerbils. *PLoS One.* 2017;12(8):e0182514.

41. Kanwal JS, Rauschecker JP. Auditory cortex of bats and primates: managing species-specific calls for social communication. *Frontiers in bioscience : a journal and virtual library.* 2007;12:4621-4640.

42. Ebadian H, Mohebbi M. Strong electric field enhancements in asymmetric metallic nanostructures and high-order harmonic generation. *Applied optics.* 2016;55(28):8035-8041.

43. Marceglia S, Foffani G, Bianchi AM, et al. Dopamine-dependent non-linear correlation between subthalamic rhythms in Parkinson's disease. *J Physiol.* 2006;571(Pt 3):579-591.

44. Coelli S, Tacchino G, Visani E, Panzica F, Franceschetti S, Bianchi AM. Higher order spectral analysis of scalp EEG activity reveals non-linear behavior during rhythmic visual stimulation. *J Neural Eng.* 2019;16(5):056028.

45. Abeysuriya RG, Rennie CJ, Robinson PA, Kim JW. Experimental observation of a theoretically predicted nonlinear sleep spindle harmonic in human EEG. *Clin Neurophysiol.* 2014;125(10):2016-2023.

46. Müller-Putz GR, Scherer R, Brauneis C, Pfurtscheller G. Steady-state visual evoked potential (SSVEP)-based communication: impact of harmonic frequency components. *J Neural Eng.* 2005;2(4):123-130.

47. Lévesque M, Salami P, Gotman J, Avoli M. Two seizure-onset types reveal specific patterns of high-frequency oscillations in a model of temporal lobe epilepsy. *J Neurosci.* 2012;32(38):13264-13272.

48. Lévesque M, Herrington R, Hamidi S, Avoli M. Interneurons spark seizure-like activity in the entorhinal cortex. *Neurobiol Dis.* 2016;87:91-101.

49. Schiff SJ, Colella D, Jacyna GM, et al. Brain chirps: spectrographic signatures of epileptic seizures. *Clin Neurophysiol.* 2000;111(6):953-958.

50. Fries P, Nikolic D, Singer W. The gamma cycle. *Trends Neurosci.* 2007;30(7):309-316.

51. G Bk. Rhythms of the brain. *New York: Oxford UP.* 2006.

52. Manning JR, Jacobs J, Fried I, Kahana MJ. Broadband shifts in local field potential power spectra are correlated with single-neuron spiking in humans. *J Neurosci.* 2009;29(43):13613-13620.

Figure Legends

Figure.1. H patterns recorded in seizures with various ictal EEG onset patterns.

A . The six ictal onset patterns on SEEG: 1.1, preictal spikes/sharps/polyspikes followed LVFA; 1.2, preictal spikes/sharps/polyspikes followed HVFA; 2, slow wave/ DC shift followed by LVFA; 3, spikes activity; 4, LVFA; 5, beta activity; 6, delta-brush.

B .The percentage of patients presenting with certain EEG onset patterns that did or did not exhibit H pattern. H pattern was present in all onset patterns except for the delta-brush.

C. EEG and corresponding TFM (top and middle) during seizures. The TFM show the proposed 'harmonic pattern (H pattern)': multiple equidistant high-density, narrow bands with changing frequency over time. The initial H patterns presented at various seizure stages on TFM. The black double arrows in the red box mark the start time point of H pattern. The power spectral density corresponding to the maximum frequency point of H pattern (the black arrow) demonstrates an equidistant distribution of the frequency bands (bottom). The frequency interval were 26、27 and 16 Hz respectively. LVFA: low-voltage fast activity; HVFA: high-voltage fast activity; TFM: time frequency maps; (Red star: seizure onset. Max Freq: maximal frequency; Min Freq: minimal frequency.

Figure.2. Two types of EEG segments harboring H pattern.

A. H pattern presented in fast activity (FA-H pattern) and irregular polyspikes (PS-H pattern). The power spectral density (bottom) at the maximum frequency point shows an equidistant distribution of the frequency bands.

B. Comparison of parameters between FA-H pattern and PS-H pattern. The former has fewer number of frequency bands, higher frequency interval， earlier start and end times, higher maximal and minimal frequencies than the latter. *$P < 0.05$; **$P < 0.01$; ***$P < 0.001$.The white arrows mark the appearance of different frequency bands. Max Freq: maximal frequency; Min Freq: minimal frequency.

Figure.3. Distribution of H pattern.

A. Anatomical distribution of SOZ, PZ and OZ in a patient (left panel). In this case, the SOZ is located precentral gyrus with early propagation to the postcentral gyrus. The right panel (B) shows the corresponding EEG recordings from the SOZ, PZ, and OZ, along with the observed H pattern. Red stars: seizures.

B. Comparison of parameters among SOZ、PZ and OZ in group data.

The distribution percentage of H pattern decreases in the order of SOZ, PZ, and OZ. The SOZ exhibit the highest number of bands, while the OZ shows the lowest maximal frequency. Max Freq: maximal frequency; Min Freq: minimal frequency. SOZ: seizure onset zone; PZ: early propagation zone; OZ: other zone.

Figure.4. Resection of dominant H pattern and surgical outcome.

A. Patients with good outcome had a significantly larger resection proportion of dominant H pattern than those with poor outcome. No such difference was seen for the SOZ. *$P < 0.05$; **$P < 0.01$; ***$P < 0.001$. *d*H pattern: dominant H pattern. SOZ: seizure onset zone.

B. Multivariate logistic regression analysis. After adjusting for potential confounders including pathology, lesional MRI, epilepsy duration, a complete resection of areas showing dominant H pattern was correlated with good surgical outcome.

Figure.5. Two representative illustrations of nonlinear analysis of *d*H and non-*d*H patterns in FA-H patterns. The left panel shows the first example: More harmonic components in *d*H pattern is due to sharper troughs of the FA waves than those in non-*d*H pattern. A/D: original SEEG signals with FA onset in *d*H/non-*d*H patterns (top), detrended SEEG signals (middle), TFM (bottom); B/E: troughs (blue circles) and peaks (red stars) of FA signals (blue lines) in *d*H/non-*d*H patterns fitted by sin waves (red lines) respectively (top), with periods T of each wave shown at middle layer, TFM of the fitting waves at bottom layer; C/F: histograms of periods (left) and trough period vs. peak period (right) of the fitted FA signals for *d*H/non-*d*H patterns.

The right panel shows the second example: More harmonic components in *d*H pattern is due to sharp extended troughs and peaks of the FA waves. G/J: original SEEG signals with FA onset in *d*H/non-*d*H patterns (top), detrended SEEG signals (middle), TFM (bottom); H/K: troughs (blue circles) and peaks (red stars) of FA

signals (blue lines) in *d*H/non-*d*H patterns fitted by sin waves (red lines) respectively (top), with periods T of each wave shown at middle layer, TFM of the fitting waves at bottom layer. As shown in middle layer, both troughs (red stars) and peaks (blue circles) are sharp with short periods than the primary period (black dashed line) of the EEG signal of *d*H pattern; I/L: enlarged plots of detrended SEEG signals and sine fitting with troughs and peaks, whose duration over periods of sine wave are shown at bottom layer. The sharp sine waves for both troughs and peaks in *d*H pattern are extended with more than half of the primary period of the EEG signal in I, which showed that the ratio of durations of both troughs and peaks over the primary period was much larger than half in I, bottom. Green dashed line in A-B, D-E and G-L represents the thresholds for extracting the periods of troughs and peaks, set as std/2 for *d*H pattern and std/3 for non-*d*H pattern. Std: standard deviation. FA is indicated as the region between two red vertical lines.

Figure.6. Two representative illustrations of nonlinear analysis of *d*H and non-*d*H patterns in FA-H pattern and PS-H pattern. The left panel shows the third example of FA-H pattern: Stronger harmonic components in *d*H pattern is due to asymmetric waveshapes. A/D: original SEEG signals with FA onset in *d*H/non-*d*H patterns (top), detrended SEEG signals (middle), TFM (bottom); B/E: troughs (blue circles) and peaks (red stars) of FA signals (blue lines) in *d*H/non-*d*H patterns fitted by sin waves (red lines) respectively (top), with periods T of each wave shown at middle layer, TFM of the fitting waves at bottom layer; C/F: enlarged plots of detrended SEEG

signals, where trough-to-peak (left blue triangle) and peak-to-trough (right red triangle) durations are compared at bottom layer. Green dashed lines in A-B and D-E are the same with those in Fig. 5. The region between two red vertical lines indicates the FA region.

The right panel shows the example of PS-H pattern: More harmonic components in *d*H pattern is due to the sharp rhythmic pulses of the PS waves, which do not exist in non-*d*H pattern. G/J: original SEEG signals in *d*H/non-*d*H patterns (top), detrended SEEG signals (middle), TFM (bottom); H/K: PS waves with/without sharp pulses in *d*H/non-*d*H patterns. Removing pulses of the PS waves in *d*H pattern (top in H) results in similar waves in *d*H and non-*d*H pattern, but larger wave amplitude (middle in H) in *d*H pattern than that (top in K) in non-*d*H pattern. Similar TFM of PS waves without pulses in *d*H (bottom in H) and non-*d*H (bottom in E) pattern. I/L: sin wave fitting (black) further reduces the harmonic components in both *d*H (bottom in I) and non-*d*H (bottom in L) patterns. Green dashed lines guide the separation of rhythmic pulses and the rest oscillations. The region between two red vertical lines indicates the PS region.

Figure.7. Distinguishing between the harmonic structures due to PAC and nonlinear effects.

A. Illustration of *d*H pattern and non-*d*H pattern in FA-H pattern (top) and corresponding power and bicoherence (middle), AAC (bottom).

B. Illustration of *d*H pattern and non-*d*H pattern in PS-H pattern (top) and

corresponding power and bicoherence (middle), AAC (bottom).

C. The region of interest (ROI) is divided according to the first three frequency bands in the bispectral plane. The diagonal represents a symmetry axis: ROIs in the lower part of the plane (squares with continuous border) are the same as ROIs in the upper part of the plane (squares with dotted border). ROIs on the diagonal are symmetrical, too. ROI1= [f_{1st}; f_{1st}]; ROI2= [f_{1st}; f_{2st}]; ROI3= [f_{1st}; f_{3st}]; ROI4= [f_{2st}; f_{2st}]; ROI5= [f_{2st}; f_{3st}]; ROI6= [f_{3st}; f_{3st}]; f_{1st}: the first frequency band, f_{2st}: the second frequency band, f_{3st}: third frequency band.

D. The maximal bicoherence comparison between *d*H pattern zone and non-*d*H pattern zone. All ROIs demonstrated higher bicoherence in *d*H pattern compared to non-*d*H pattern, except for ROI1.

PAC: phase-amplitude coupling; AAC: amplitude-amplitude coupling.

Figure 1

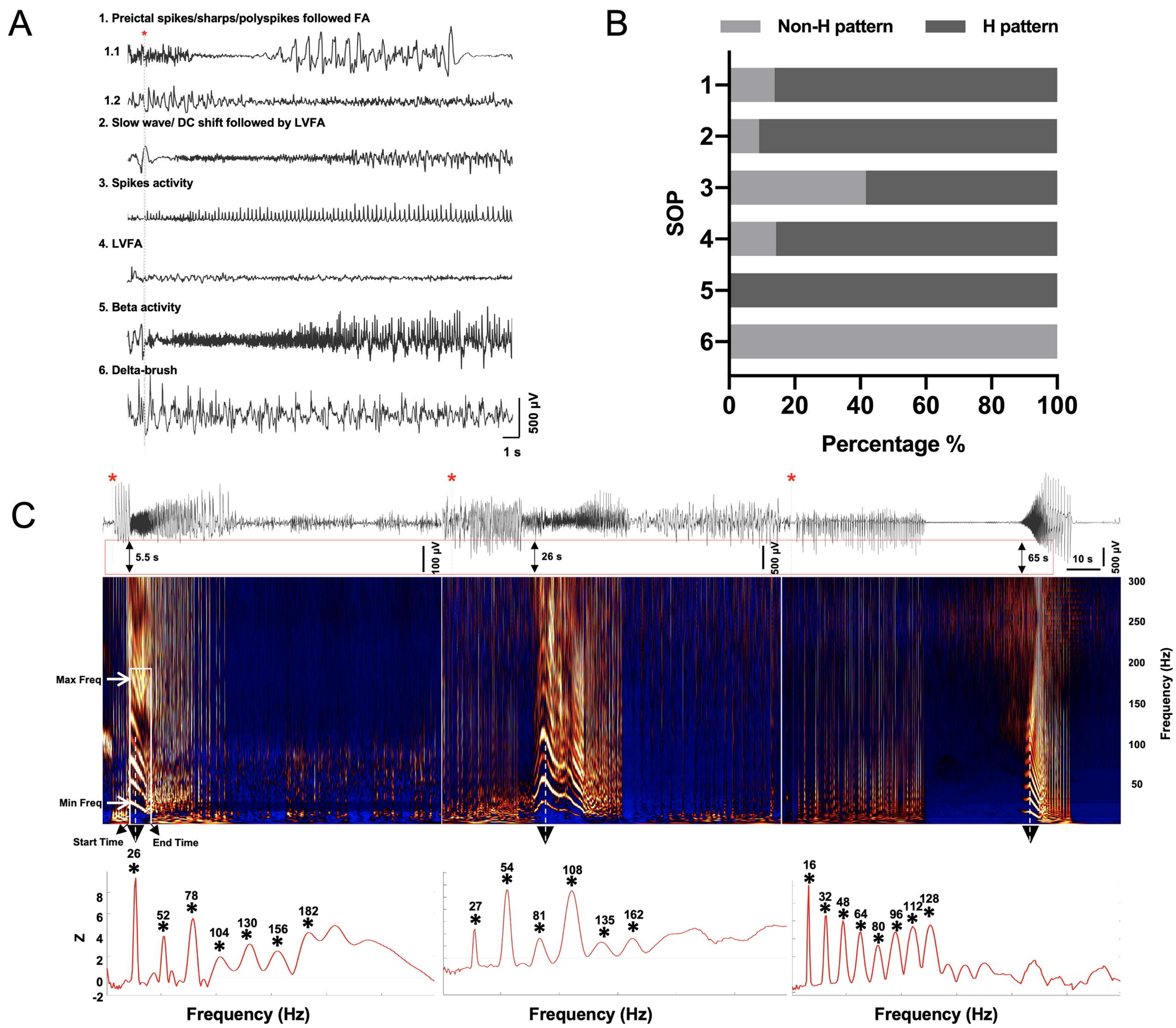
A
1. Preictal spikes/sharps/polyspikes followed FA
1.1
1.2
2. Slow wave/ DC shift followed by LVFA
3. Spikes activity
4. LVFA
5. Beta activity
6. Delta-brush
500 µV
1 s
B
Non-H pattern
H pattern
SOP
1
2
3
4
5
6
0
20
40
60
80
100
Percentage %
C
5.5 s
100 µV
26 s
500 µV
65 s
10 s
500 µV
Max Freq
Min Freq
Start Time
End Time
Frequency (Hz)
300
250
200
150
100
50
Z
8
6
4
2
0
-2
26
52
78
104
130
156
182
27
54
81
108
135
162
16
32
48
64
80
96
112
128
Frequency (Hz)
Frequency (Hz)
Frequency (Hz)

Figure 2

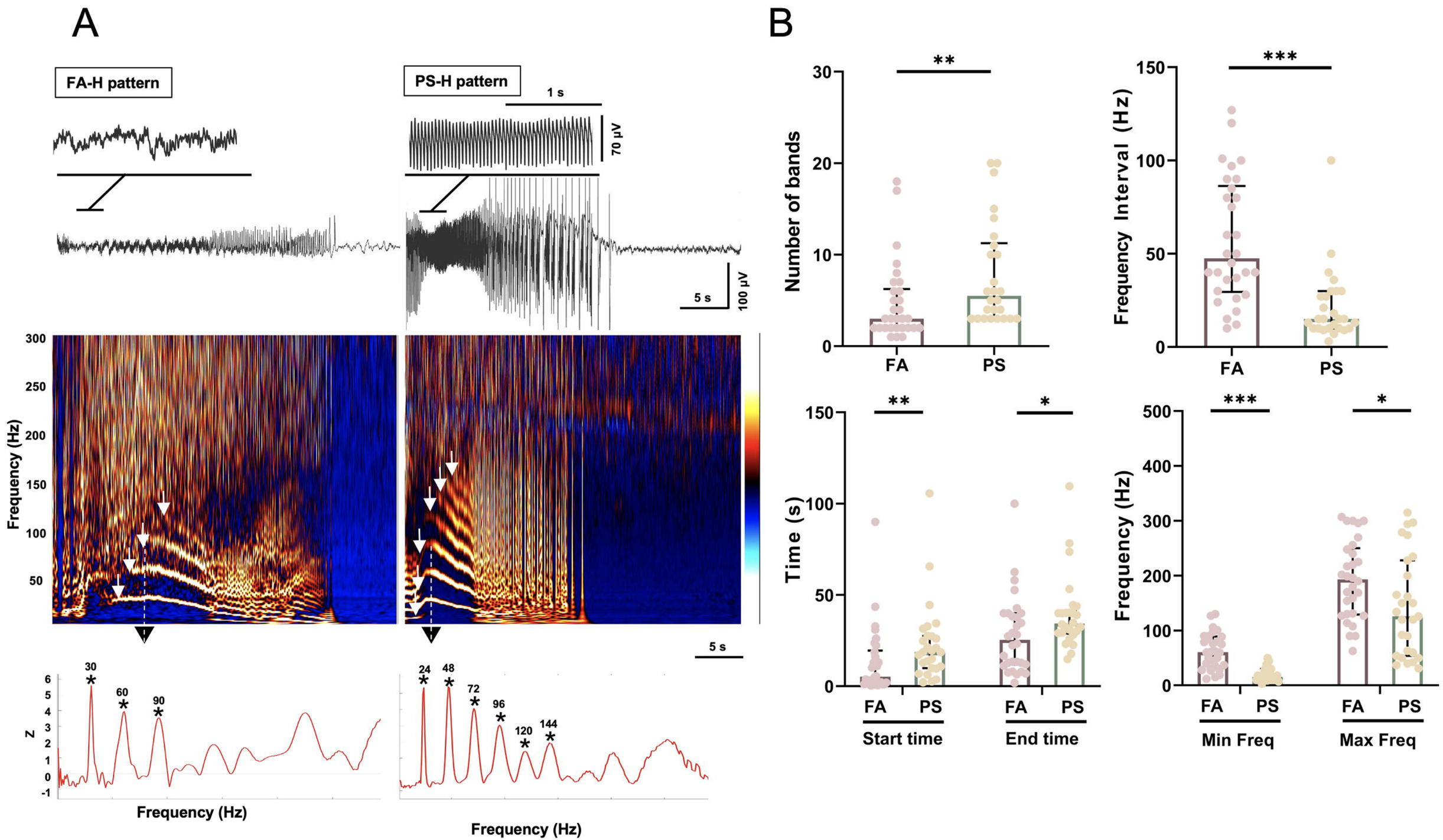
A
FA-H pattern
PS-H pattern
1 s
70 µV
5 s
100 µV
Frequency (Hz)
300
250
200
150
100
50
5 s
30
60
90
24
48
72
96
120
144
Z
Frequency (Hz)
Frequency (Hz)
B
Number of bands
Frequency Interval (Hz)
Time (s)
Frequency (Hz)
FA
PS
Start time
End time
Min Freq
Max Freq
**
***
*

Figure 3

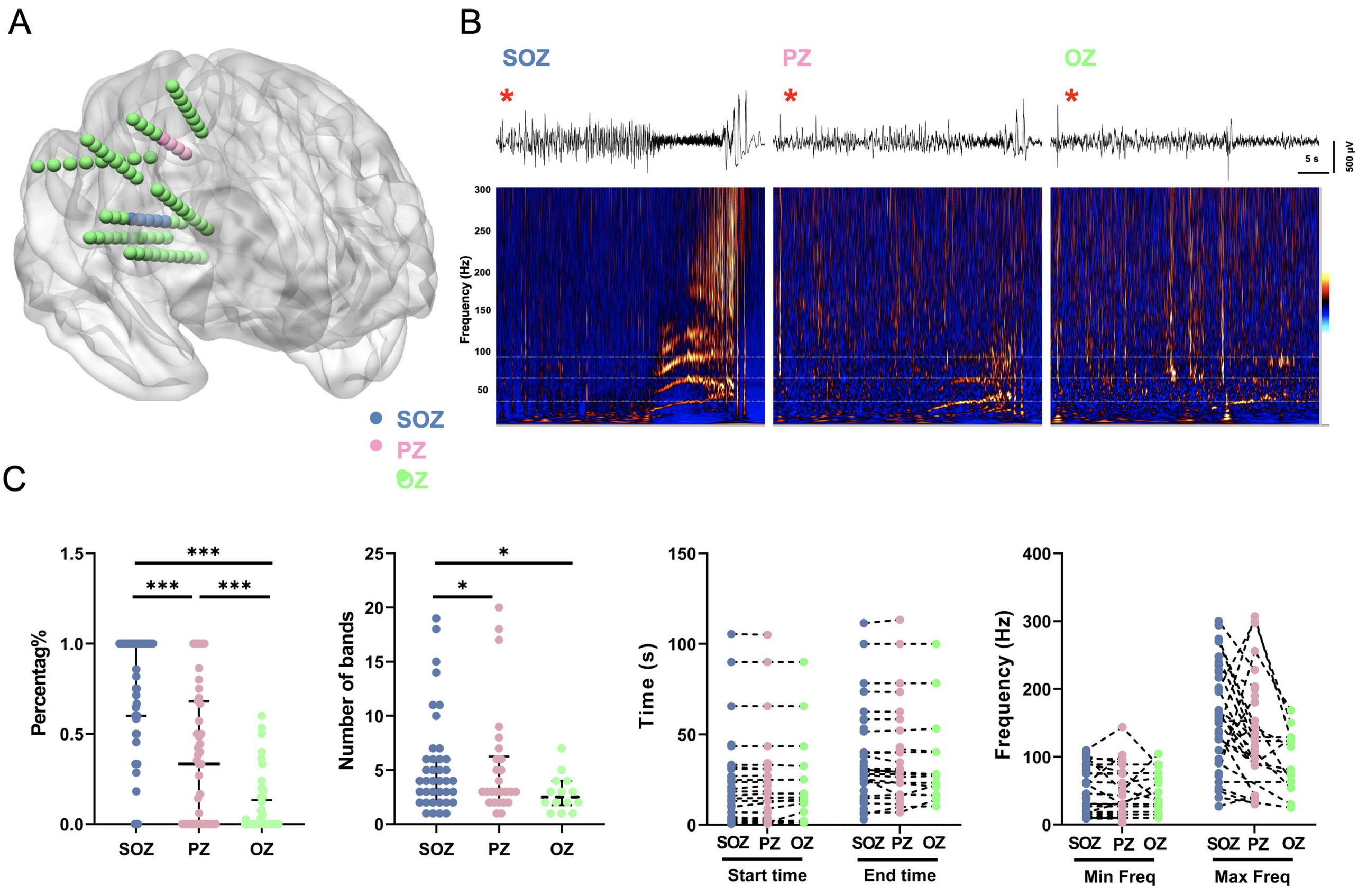
A
SOZ
PZ
OZ
B
SOZ
PZ
OZ
5 s
500 µV
Frequency (Hz)
300
250
200
150
100
50
C
Percentag%
1.5
1.0
0.5
0.0
***
***
***
SOZ
PZ
OZ
Number of bands
25
20
15
10
5
0
*
*
Time (s)
150
100
50
0
SOZ PZ OZ
Start time
End time
Frequency (Hz)
400
300
200
100
0
Min Freq
Max Freq

Figure 4

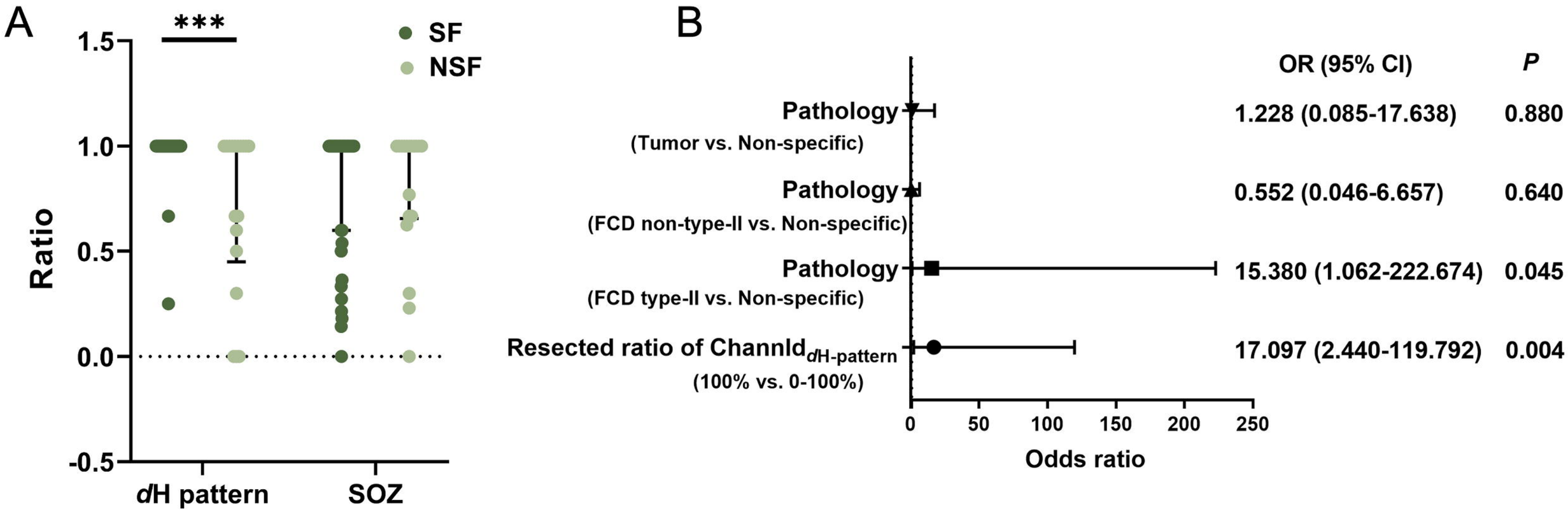
A
***
SF
NSF
1.5
1.0
0.5
0.0
-0.5
Ratio
dH pattern
SOZ
B
OR (95% CI)
P
Pathology
(Tumor vs. Non-specific)
1.228 (0.085-17.638)
0.880
Pathology
(FCD non-type-II vs. Non-specific)
0.552 (0.046-6.657)
0.640
Pathology
(FCD type-II vs. Non-specific)
15.380 (1.062-222.674)
0.045
Resected ratio of ChannId dH-pattern
(100% vs. 0-100%)
17.097 (2.440-119.792)
0.004
0
50
100
150
200
250
Odds ratio

Figure 5

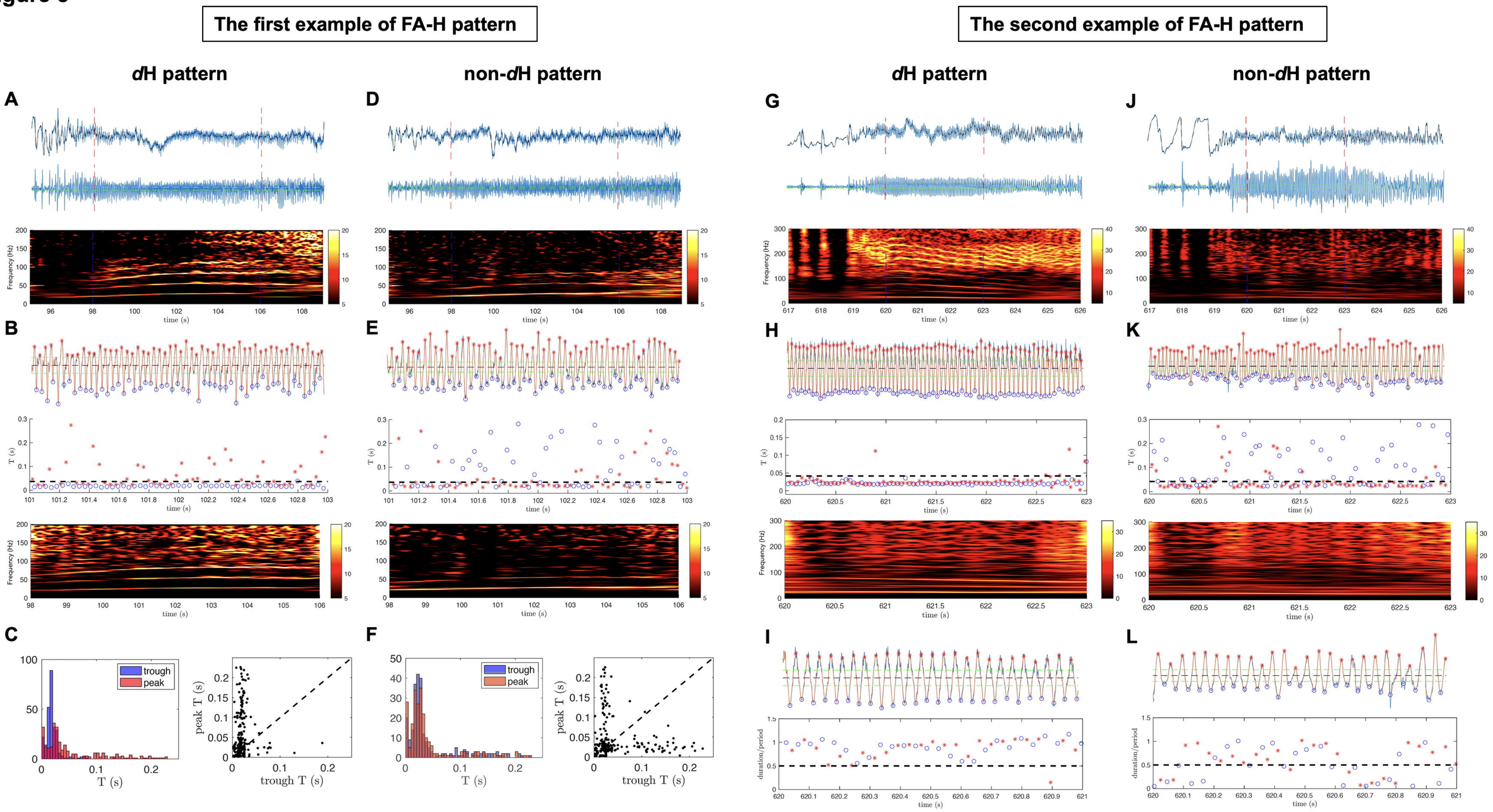
The first example of FA-H pattern
The second example of FA-H pattern
dH pattern
non-dH pattern
dH pattern
non-dH pattern
A
B
C
D
E
F
G
H
I
J
K
L
Frequency (Hz)
time (s)
T (s)
trough
peak
peak T (s)
trough T (s)
duration/period

Figure 6

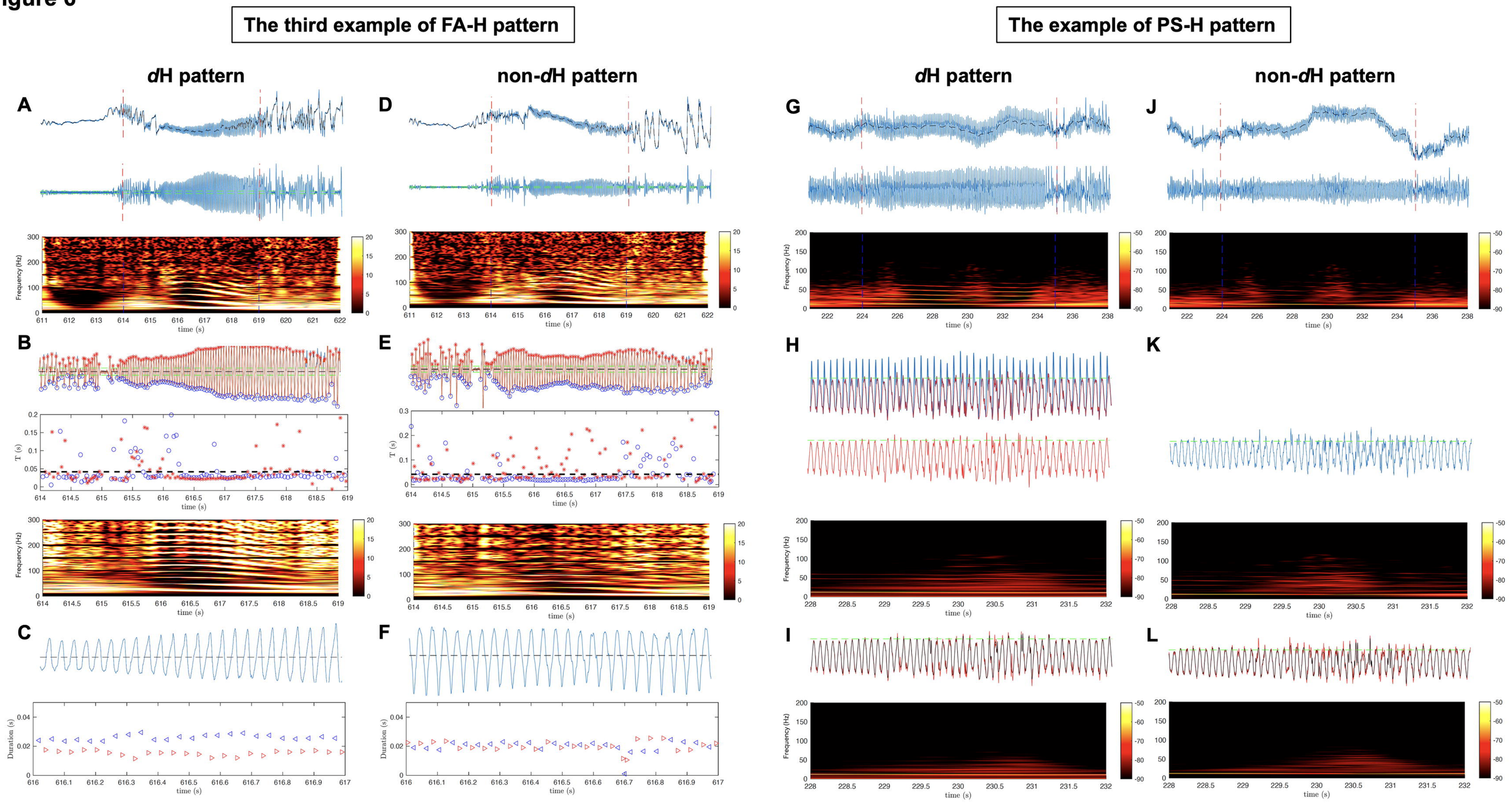
The third example of FA-H pattern
The example of PS-H pattern
dH pattern
non-dH pattern
dH pattern
non-dH pattern
A
B
C
D
E
F
G
H
I
J
K
L
Frequency (Hz)
T (s)
Duration (s)
time (s)

Figure 7

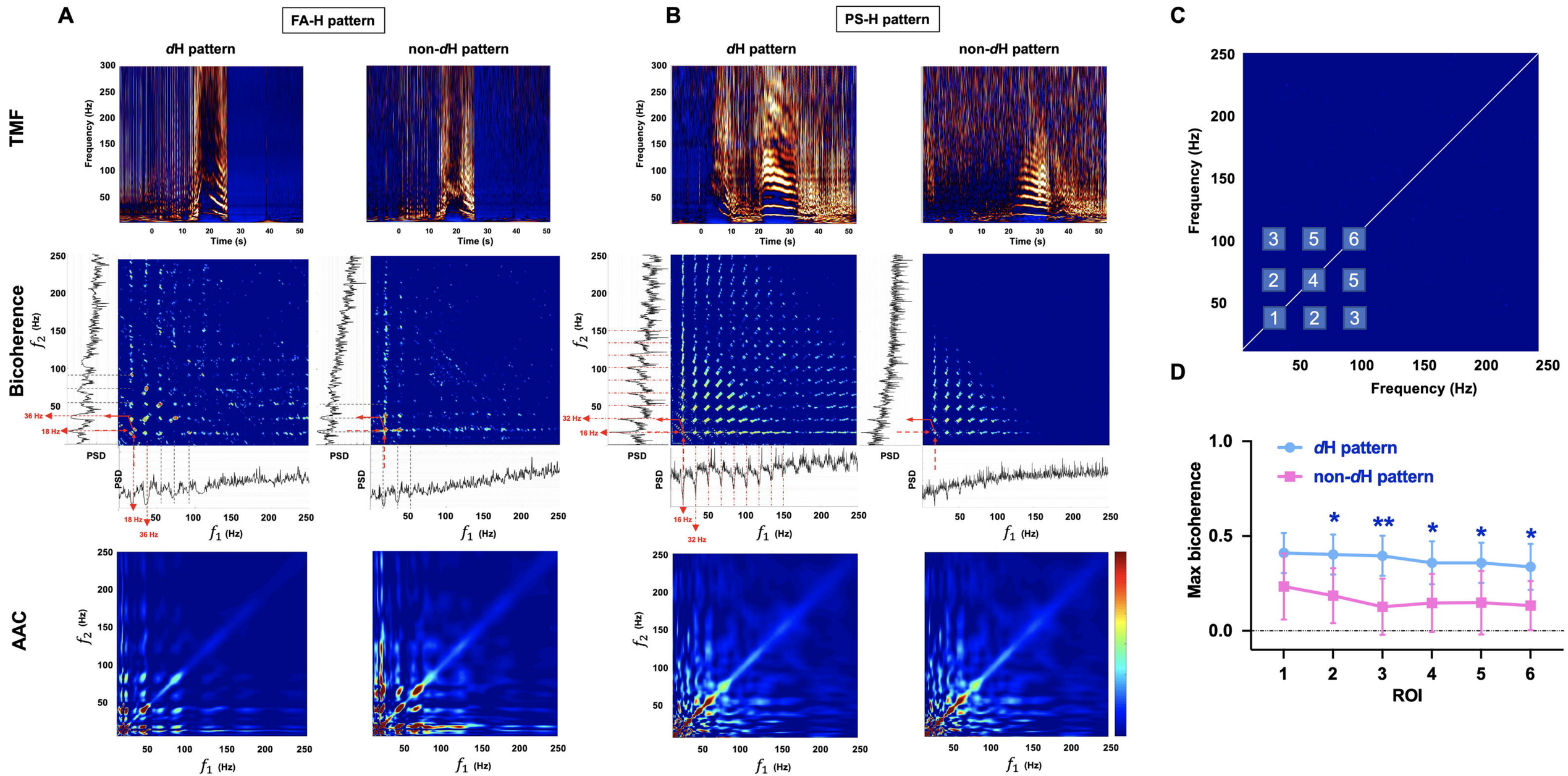
A
FA-H pattern
dH pattern
non-dH pattern
B
PS-H pattern
dH pattern
non-dH pattern
C
D
TMF
Bicoherence
AAC
Frequency (Hz)
Time (s)
PSD
f_1 (Hz)
f_2 (Hz)
36 Hz
18 Hz
32 Hz
16 Hz
Max bicoherence
ROI
dH pattern
non-dH pattern

Table 1. Clinical characteristics and surgical outcome in the patients with focal onset pattern on iEEG

	Total (n = 57)	**Engel class Ia (n = 39)**	**Engel class > Ia (n = 18)**	***P* value**
Gender, M, n (%)	31 (54.4 %)	20 (51.3 %)	11 (61.1 %)	0.574
Age at onset, y	10.4±8.5	9.4±7.5	12.6±10.2	0.193
Age at surgery, y	23.6±12.3	23.6±12.8	23.7±11.3	0.991
Epilepsy duration, y	13.3±11.2	14.2±11.8	11.1±9.6	0.329
EEG segments with H pattern, FA/PS	30/27	20/19	10/8	0.784
Lateralization, L, n (%)	26 (45.6 %)	18 (46.2 %)	8(44.4 %)	1.000
Contact number	94.7±29.1	86.5±22.9	112.5±33.4	0.262
Epileptogenic lesion on MRI, n (%)	49 (85.9 %)	35 (89.7 %)	14 (77.8 %)	0.414
Localization, n (%)				0.208
Temporal	20 (35.1 %)	10 (25.6 %)	10 (55.6 %)	
Frontal	24 (42.1 %)	18 (46.2 %)	6(33.3 %)	
Parietal	4(7.0 %)	3 (7.7 %)	1(5.6 %)	
Occipital	4(7.0 %)	4(10.3 %)	0(0.0 %)	
Multi-lobar	5(8.8 %)	4(10.3 %)	1(5.6 %)	
Pathology, n (%)				0.003
Hippocampal sclerosis	6(10.5 %)	5 (12.8 %)	1 (5.6 %)	
Focal cortical dysplasia type II	28 (49.1 %)	23 (59 %)	5 (27.8 %)	
Focal cortical dysplasia (non-type II)	11 (19.3 %)	7(17.9 %)	4 (22.2 %)	
Tumor	2 (3.5 %)	2(5.1 %)	0(0.0 %)	
Others	10 (17.5%)	2 (5.1 %)	8 (44.4 %)	

Abbreviations: M: male; y: years; H pattern: harmonic pattern; FA: fast activity; PS: periodic spike; L: left; MRI: magnetic resonance imaging. Data are presented as the number of patients for categorized variables and the mean ± standard deviation for continuous variables.